Passive neutron albedo reactivity measurements of spent nuclear fuel

Tupasela, Topi

2021-01-11

1   **Passive Neutron Albedo Reactivity Measurements of Spent Nuclear Fuel**

2

3   Topi Tupasela[1], Peter Dendooven[2], Stephen J. Tobin[3], Vladyslav Litichevskyi[2], Pirkitta Koponen[2], Asko

4   Turunen[4], Mikael Moring[1], Tapani Honkamaa[1*]

5   [1]STUK – Radiation and Nuclear Safety Authority, P.O. BOX 14, FI-00811 Helsinki, Finland

6   [2]Helsinki Institute of Physics, University of Helsinki, Finland

7   [3]Los Alamos National Laboratory, Los Alamos, NM 87544, USA

8   [4]Provedos Oy, Laippatie 4b, FI-00880 Helsinki, Finland

9   *tapani.honkamaa@stuk.fi, P.O. BOX 14, FI-00811, Helsinki Finland

10

11

12   ## Abstract

13   The upcoming disposal of spent nuclear fuel in Finland creates new challenges for nuclear safeguards.

14   Part of the national safeguards concept for geological repositories, developed by STUK – Radiation and

15   Nuclear Safety Authority, is non-destructive assay (NDA) verification of all fuel items before disposal.

16   The proposed verification system is a combination of PGET (Passive Gamma Emission Tomography),

17   PNAR (Passive Neutron Albedo Reactivity) and weight measuring NDA-instruments. PGET takes a pin-

18   level image of the fission products inside of a fuel assembly and PNAR verifies the multiplication of the

19   assembly, a quantity that correlates with the fissile content. PGET is approved by IAEA (International

20   Atomic Energy Agency) for safeguards measurements, but the feasibility of PNAR has not yet been

21   established. A first of its kind PNAR prototype instrument was built in a collaboration coordinated by

22   STUK. This paper concludes the results of the first measurements of spent BWR (Boiling Water Reactor)

23   nuclear fuel with the prototype in July 2019. Based on the measurements, the ability of the PNAR

24   instrument to detect the presence of fissile material in a repeatable manner in a reasonable amount of

25   time was demonstrated. Furthermore, the instrument was able to detect differences in multiplication

26   between partially and fully spent fuel assemblies, and axial differences in multiplication within a single

27   assembly.

28

29   Keywords: PNAR, Non-destructive assay, nuclear safeguards, spent nuclear fuel

30

Passive Neutron Albedo Reactivity Measurements of Spent Nuclear Fuel

31 **1   Introduction**

32 In order to identify and prepare for challenges related to the upcoming geological disposal of spent

33 nuclear fuel in Finland, STUK - Radiation and Nuclear Safety Authority, has developed a national

34 concept for nuclear safeguards of geological repository [1]. STUK considers one of the most important

35 aspects of safeguarding the disposal is maintaining a trustworthy record of what was disposed of

36 because accessing fuel becomes extremely difficult after it is encapsulated and disposed of.

37 The national concept features verification of the declaration of all spent fuel items prior to encapsulation

38 and disposal, using the best available technology. Currently, STUK considers the best available

39 technology to be a combination of NDA techniques: PGET (Passive Gamma Emission Tomography) and

40 PNAR (Passive Neutron Albedo Reactivity) accompanied by a weight measurement. PGET takes a

41 tomographic image of the fuel assembly, from which a pin-to-pin layout of the assembly can be

42 reconstructed [2–4]. PNAR uses the neutrons radiating from the spent fuel itself to assess the

43 multiplication of the assembly. Additionally, the current PNAR design simultaneously collects signals of

44 the gross gamma and total neutron emission rates of the fuel assembly in a similar manner that is used

45 in well-established Fork detectors. Automated real-time Fork detector data analysis software developed

46 by Euratom [5] is capable of verifying that the gross gamma and total neutron count rates are consistent

47 with the operator's declaration for a specific fuel item. The same software is expected to be applicable to

48 the signals collected by PNAR. PGET also includes neutron detectors and performs a gross gamma

49 measurement. However, the detector types and designs are different than those of the PNAR. PGET

50 and PNAR were selected to complement each other because, while individual missing pins can be

51 identified in a PGET image, PNAR simultaneously verifies that the assembly contains fissile material.

52 The mixture of different signals collected by both instruments would be extremely difficult to imitate with

53 a substitute material.

54 The PNAR technique is based on two relative measurement configurations – often named high and low

55 multiplying configurations. In the high multiplying configuration, a fuel assembly is positioned in a

56 medium that reflects neutrons back into the assembly. These, thermalized, albedo neutrons can induce

57 additional fissions inside the fuel. For the instrument designed by STUK, this reflecting medium is the

58 water of a fuel storage pool. In the low multiplying configuration, the reflection of neutrons back into the

59 fuel assembly is suppressed. When the neutron reflection is suppressed, the reduction of fissions

60 caused by the albedo neutrons leads to a decrease in neutron generation rate and subsequently to a

61 decrease in the flux of neutrons escaping the system – a change which can be measured. The ratio of

62 the measured neutron flux in the two configurations, high multiplication divided by low multiplication, is

63 called the PNAR Ratio and is a measure of the multiplication in the fuel assembly for which the fissile

64 content creates the chain reaction. The PNAR concept was originally proposed in 1982 by Lee and

65 Lindquist [6] and the method has recently been discussed in more detail in several publications [7–10].

66 STUK, in collaboration with Encapsulation NDA Services, the Helsinki Institute of Physics and Provedos

67 Oy, designed and built a prototype PNAR instrument [8,11]. The prototype was designed to assay the

68 spent BWR fuel from the Finnish Olkiluoto 1 and 2 Power Plants operated by Teollisuuden Voima Oyj

69 (TVO). This type of fuel is expected to be disposed of first in Finland. The instrument is used in the fresh

70 water pool, where the spent fuel is held for interim storage. The low multiplying configuration in the

71 otherwise well-reflecting environment is achieved by surrounding the fuel assembly with a cadmium liner.

72 Cadmium has an extremely high absorption cross section for thermal neutrons. The prototype was used

73 for fuel measurements for the first time in July 2019.

74 Section 2 describes the technical design of the prototype PNAR instrument. Section 3 introduces the

75 measurement campaign of July 2019 together with the measurement results. Also, the repeatability of

76 the PNAR measurement is studied. In Section 4, the measurement results are discussed and compared

77 to previous simulated PNAR responses. Also, for one selected fuel assembly, the simultaneously

78 measured PNAR and PGET signals are compared.

79 **2   Materials and Methods**

80 A four-meter-tall support structure was built for the PNAR prototype. The support structure was designed

81 to stand on its own at the bottom of the spent fuel storage pool. The support structure includes a fuel

82 guide, that ensures the fuel assembly is safely placed in a controlled, repeatable measurement location.

83 The assembly is lowered into the fuel guide using the fuel transport machine. The inside dimensions of

84 the fuel guide were chosen to be identical to those of the fuel storage rack. A PGET device can be

85 mounted on the same support structure, on top of the PNAR instrument.

86 A cross-sectional image of the PNAR instrument is shown in Figure 1. The PNAR instrument consists of

87 four identical rectangular measurement pods. The polyethylene pods are arranged into a square, leaving

88 an opening for the fuel assembly in the middle. Each measurement pod houses one xenon-filled

89 ionization chamber for gamma measurements and one ^{3}He proportional cylindrical neutron detector. The

90 detectors are centred around the square opening and are oriented parallel to the nearest exterior side of

91 the fuel assembly. The neutron detectors are encapsulated in polyethylene cylinders which are

92 completely covered with cadmium, making the detectors sensitive to fast and epithermal neutrons. Lead

93 shielding is used to reduce the gamma radiation reaching the neutron detectors.

94 The neutron detectors contain ^{3}He gas at 6 atm. pressure. The active length of each detector is 15.5 cm.

95 In laboratory measurements, the factorial dead-time of the neutron detectors was estimated to be about

96 6% at 50 000 counts/s. The instrument was designed for gamma and neutron radiation levels of

97 assemblies that are cooled for at least 20 years before disposal and with a maximum burnup of 58

98 GWd/tU. The neutron flux for fuel assemblies that have cooled for at least 20 years is estimated to result

99 in a detector response of less than or equal to 10 000 count/s [11].

100 Each detector pod is connected to a separate counting electronics unit with 13 m long cables. The units

101 house the electronics and high voltage sources for both the ionization chamber and the neutron detector

102 of the corresponding pod. Although the PNAR Ratio is calculated from the total signal, using separate

103 counting units allows for individual control of each detector pod and the collection of distinguishable

104 signals from each detector which can be useful e.g. for troubleshooting.
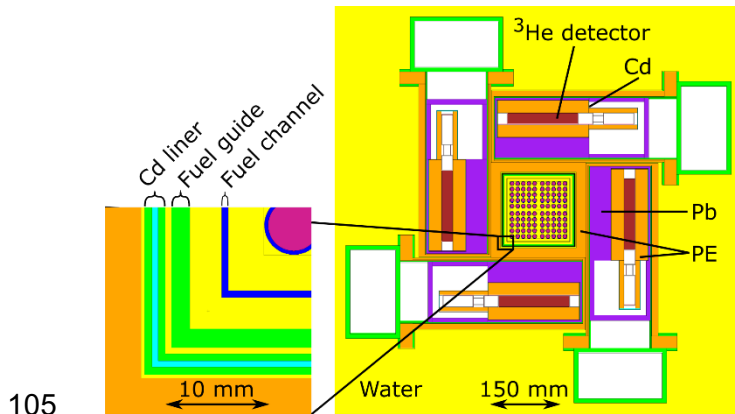
105

106 **Figure 1: Top view of the PNAR instrument design.** A fuel assembly is located in the middle of four

107 identical detector pods. When the cadmium liner is not present, water occupies that region.

108 To alternate between the high and low multiplying configurations, a movable cadmium liner is located

109 between the fuel guide channel and the central opening of the PNAR instrument. The liner for the

110 prototype was moved manually by pulling a chain from the poolside. The correct vertical position of the

111 liner was confirmed during measurements with an underwater camera. Figure 2 shows the two liner

112 positions viewed by the underwater camera.

113 The liner is built from four 0.5 mm thick, 50 cm tall and 30 cm wide cadmium sheets, each bent in the

114 middle into a 90-degree angle along the longest axis. These sheets are assembled into a 50 cm tall

115 rectangular box, where the adjacent cadmium sheets overlap each other for 10 cm length on each side.

116 This assembly is encapsulated between two 1.2 mm thick, 55 cm long stainless-steel square tubes

117 which are then welded shut at both ends to isolate the cadmium from the environment. The location of

118 the cadmium layer was verified by X-ray scanning of the final liner. The small water gap in which the

119 cadmium liner moves between the PNAR pods and the fuel guide channel is highlighted in Figure 1.

120
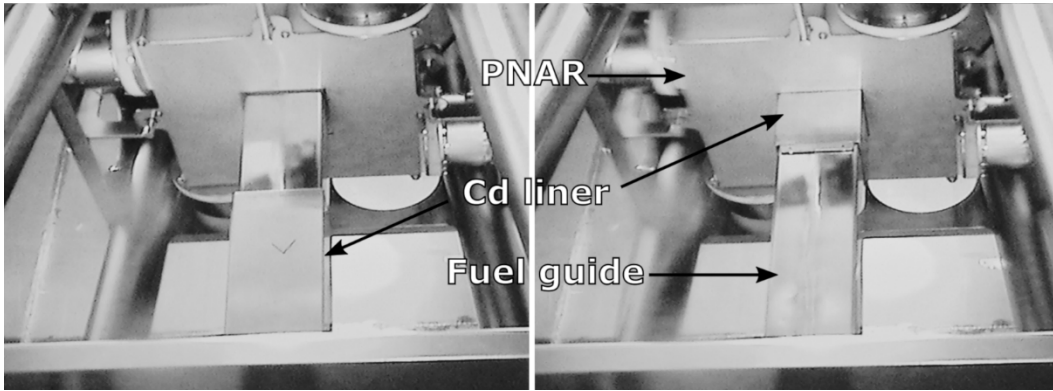
Figure 2: Movement of the cadmium liner. The cadmium is completely encapsulated inside a stainless-steel cover. Viewed from below the PNAR instrument, the movement of the cadmium liner over the fuel guide between the two measurement configurations can be seen. **Left:** Cadmium liner in the high multiplying configuration. **Right:** Cadmium liner in the low multiplying configuration. Pictures: TVO

3   Results

A measurement campaign was held in July 2019 in the interim spent fuel storage facility in Olkiluoto, where spent fuel from the Olkiluoto nuclear power plant is stored in fresh water storage pools. A PGET instrument was mounted above the PNAR instrument on the same support structure, and measurements were taken simultaneously with both devices. Pictures of the measurement system during the campaign are shown in Figure 3. A total of 23 assemblies were measured. The measured assemblies were selected to represent multiple fuel designs and irradiation histories. The assemblies, together with declared average burnup, cooling time and average initial enrichment are listed in Table 1.

Table 1: Measured assemblies and the measured PNAR Ratios and average gross neutron and gamma signals at the default measurement height. For the assemblies measured from two heights, the PNAR Ratio at the higher measurement position and the difference with the standard measurement position (in brackets) are also listed. The quoted uncertainties represent the standard deviations associated to counting statistics.

Assembly #	Assembly type	IE (%)	BU (GWd /tU)	CT (a)	PNAR Ratio	PNAR Ratio +150 cm	Neutron detector count rate (cts/s)	Gross gamma signal (a.u.)
1	8x8-1	1.9	19	35	**1.0422 ±0.0026**	-	700	92740
2	8x8-1	2.9	31	29	**1.0397 ±0.0017**	-	3190	176200
3	SVEA-64	3.0	34	21	**1.0427 ±0.0011**	-	7777	279400
4	SVEA-64	3.0	38	21	**1.0443 ±0.0009**	**1.0573 ±0.0009** (+0.0130 ±0.0013)	10790	298500
5	SVEA-64	3.0	20	23	**1.0883 ±0.0032**	-	970	163300
6	SVEA-64	3.0	33	20	**1.0492 ±0.0011**	-	7195	278900
11	SVEA-64	3.0	33	21	**1.0476 ±0.0012**	-	6767	271800
13	SVEA-64	3.0	36	21	**1.0451 ±0.0010**	-	9322	293600

18	9x9-1AB	3.2	35	23	**1.0376 ±0.0012**	-	6349	246700
20	ATRIUM10	3.2	37	17	**1.0495 ±0.0009**	**1.0531 ±0.0010** (+0.0036 ±0.0013)	10250	312900
22	SVEA-100	3.2	38	19	**1.0441 ±0.0010**	-	8740	300600
23	SVEA-64	3.0	34	21	**1.0445 ±0.0010**	-	8517	281600
24	SVEA-64	3.0	33	21	**1.0445 ±0.0010**	-	6473	270400
28	SVEA-64	3.0	33	21	**1.0465 ±0.0010**	-	6230	251000
30	9x9-1AB	3.2	35	21	**1.0457 ±0.0012**	-	6246	253200
31	9x9-1AB	3.2	36	21	**1.0423 ±0.0012**	-	6084	251800
35	Optima	3.2	40	14	**1.0464 ±0.0008**	**1.0631 ±0.0010** (+0.0167 ±0.0012)	15690	394100
39	ATRIUM10	3.2	35	17	**1.0536 ±0.0011**	**1.0534 ±0.0010** (-0.0001 ±0.0015)	7796	293000
42	GE12	3.2	36	17	**1.0452 ±0.0011**	**1.0436 ±0.0006** (-0.0016 ±0.0011)	8771	304500
43	GE12	3.2	43	12	**1.0386 ±0.0006**	**1.0372 ±0.0007** (-0.0014 ±0.0010)	18451	401900
44	GE14	3.5	42	10	**1.0443 ±0.0007**	**1.0496 ±0.0008** (+0.0053 ±0.0010)	20790	472100
46	GE14	3.5	43	6	**1.0490 ±0.0006**	**1.0508 ±0.0007** (+0.0018 ±0.0009)	23960	653900
49	ATRIUM10	3.6	50	11	**1.0306 ±0.0005**	**1.0394 ±0.0006** (+0.0088 ±0.0008)	30160	492100

138

139 The lengths of all the selected assemblies are within a few centimetres from each other. They were
140 measured at a default measurement height of approximately 1.4 m from the bottom of the assembly to
141 the centre level of the neutron detectors. Additionally, several assemblies were measured at a position
142 1.5 m above the default location. One assembly was measured at 7 different heights. Positioning
143 uncertainty was quantified by sets of repeated measurements on four different assemblies, where the
144 assembly was rotated 90 degrees in between the measurements.
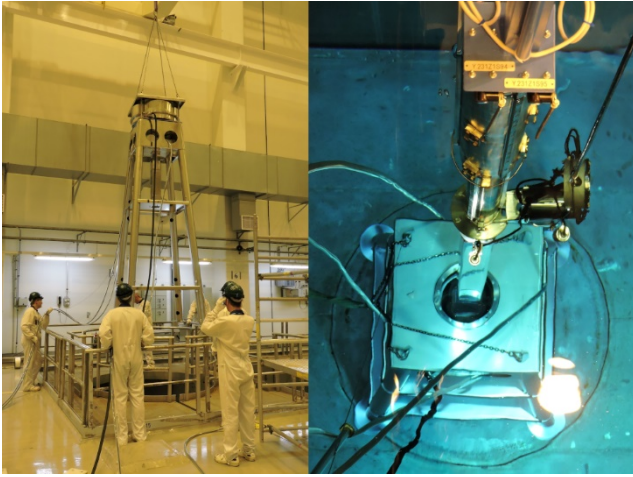
145

146 **Figure 3: Measurement system operation. Left:** Complete PNAR-PGET measurement system within

147 the common support structure being moved into the fuel storage pool. **Right:** An assembly in the

148 measurement position at the bottom of the storage pool. Pictures: TVO

149 One of the detector pods was unusable throughout the measurement campaign. The reason for

150 malfunctioning was a water leak, which was identified after the device was lifted from the pool after the

151 campaign. To preserve symmetry, all the reported PNAR Ratios are quantified using the signals of the

152 two working opposite pods. Thus, the total amount of counts gathered in each measurement was

153 effectively halved from the expected scenario. The data collecting time was approximately 120 seconds

154 for both the measurements with and without cadmium liner.

155 **3.1   PNAR Ratios and gross gamma intensity**

156 Table 1 lists all the measured assemblies and the PNAR Ratios measured at the default measurement

157 height together with statistical uncertainties. The standard deviation of each individual counting

158 measurement is the square root of the total counts. Through propagation of uncertainty, the standard

159 deviation of the PNAR Ratio, σ_{PNAR}, can be calculated as

160
$$\sigma_{PNAR} = PNAR\ Ratio * \sqrt{N_{high}^{-1} + N_{low}^{-1}},$$

161 where N_{high} and N_{low} are the total measured counts for high and low multiplication measurements,

162 respectively. For the assemblies that were measured from 2 heights, the PNAR Ratio at the higher

163 position is reported together with the absolute difference, and its uncertainty, compared to the default

164 position in Table 1.

165 Table 1 also lists the measured average neutron count rate and gamma intensity summed over the two

166 opposite detectors in the high multiplying configuration. The detector responses were not calibrated to

167 any known source and are meant to be interpreted as relative values only. The neutron detector bias

168 (1560 V) was selected so that the detector works in proportional region for all the measured assemblies.

169 This was confirmed with bias voltage scans for assemblies #20 and #46, which are shown in Figure 4.

170 The ion chamber bias was set at -500 V based on laboratory experiments performed before the

171 campaign. No calibration measurements were done to assure the linearity of the gamma detector

172 response during the measurement campaign.
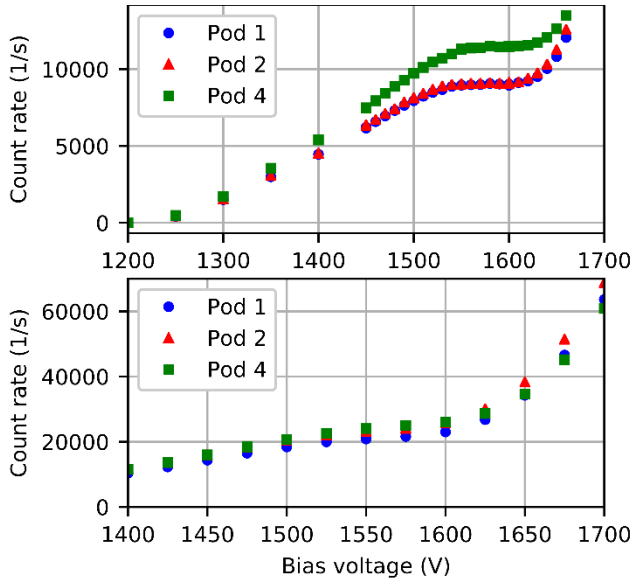
173

174 **Figure 4: Neutron detector bias voltage scan for assemblies #20 (Above) and #46 (Below).** Bias

175 voltage scans were performed to select a bias voltage for the neutron detectors such that they operate in

176 the proportional region. Assembly #20 was selected to resemble the most intense assemblies from a

177 gamma ray perspective to be disposed of in the geological repository. Assembly #46 had the highest

178 gamma intensity of the measured assemblies. The plateau is still, but barely, noticeable. Based on the

179 scans, the bias voltage was set to 1560 V for subsequent measurements.

180 In Figure 5, the measured assemblies are divided into 4 initial enrichment (IE) groups and the PNAR

181 Ratios at the default measurement height are plotted against the assembly burnup. Most of the

182 assemblies have a PNAR Ratio between 1.03 and 1.05. The initial enrichment expresses the fissile

183 material content averaged over the entire fresh fuel assembly. As the fuel is used (burnup increases),

184 the fissile material content depletes, and fission products and actinides are produced. Higher burnups

185 can be achieved for assemblies with higher initial enrichment. From an economical point of view, it is

186 desirable for the operator to deplete the fuel as much as possible. Thus, most of the discharged

187 assemblies are expected to have similar multiplication values and consequently similar PNAR Ratios as

188 observed in Figure 5. One measured assembly (#5) had a low burnup (20 GWd/tU) compared to its initial

189 enrichment (3.0 %). This assembly is considered only partially burned, which can be also seen from the

190 significantly higher PNAR Ratio of 1.0883 ± 0.0032. Another assembly (#1) with similar low burnup was

191 also measured. However, this assembly had low initial enrichment of 1.9 % and had a PNAR Ratio that

192 matches the other fully depleted assemblies. It is expected that cooling time will have an impact on the

193 multiplication of each assembly as the isotopic content of each assembly evolves with time. Yet, the

194 cooling time dependence is not expected to be as strong a dependence as the initial enrichment and

195 burnup dependences. This is supported by a study within the Next Generation Safeguards Initiative

196 [12,13], which shows, for various assemblies, that the dependence of multiplication on cooling time is

197 small within the cooling time range of the work presented here.

198 Based on MCNP6.2 [14] simulations of PNAR response to fuel with fission events turned off, i.e. fuel

199 where each fission reaction is terminated as an absorption, a non-multiplying fuel assembly would have

200 a PNAR Ratio of 0.97. This result is an approximation because simulation does not necessary reflect the

201 reality accurately. There is no real way to measure the response of a non-multiplying fuel assembly. The

202 ratio is below 1 because in the low multiplying configuration the cadmium liner displaces water between

203 the assembly and the detectors, a change which increases the detection efficiency for the high energy

204 neutrons that the STUK PNAR detector was designed to detect. In Figure 5, the vertical axis is cut at

205 0.97. The PNAR Ratio gap between the PNAR Ratios of typical fully irradiated assemblies and the

206 PNAR Ratio of a non-multiplying assembly is the dynamic range of a PNAR instrument. This dynamic

207 range is also expressed in Figure 5.
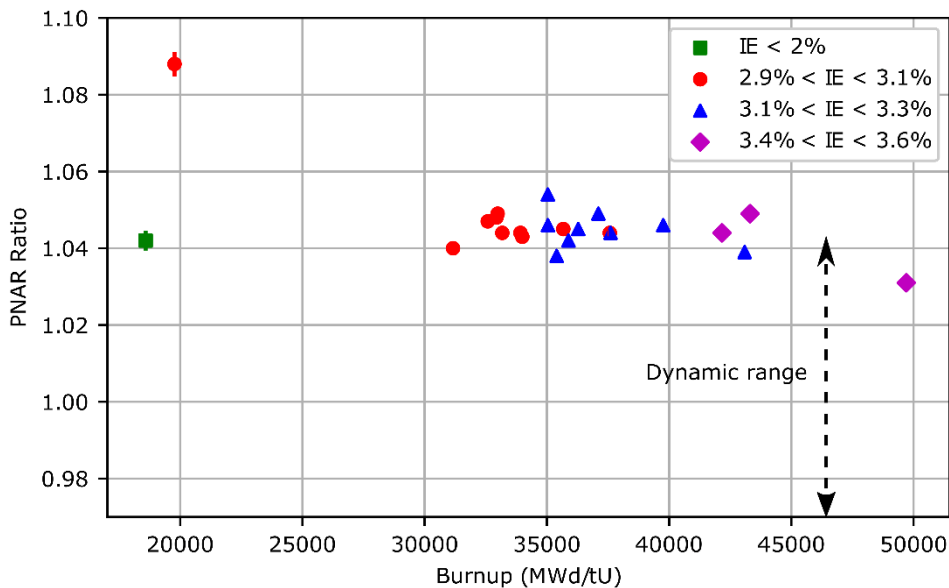
208

209 **Figure 5: Measured PNAR Ratios as a function of assembly burnup.** The measured assemblies are

210 grouped based on their initial enrichment (IE). The 1 standard deviation error bars are smaller than the

211 markers for most data points.

212 **3.2 Measurement repeatability**

213 The repeatability of the PNAR measurement was tested by performing repeated measurements. Four

214 assemblies were measured four separate times for a total of 16 measurements. Between each

215 measurement, the assembly was lifted out of the detector, rotated over 90 degrees and lowered back

216 into the measurement position. The mean of the four measurements, per assembly, was taken as the

217 best estimation for the true PNAR Ratio of an individual assembly. The individual measurement results,

218 the mean values and the standard errors of the mean values are reported in Table 2. The one standard

219 deviation uncertainties of the measured PNAR Ratios are calculated in the same way as described in

220 Chapter 3.1. The deviations of the single measurements from the mean PNAR Ratio of the

221 corresponding assembly are shown in Figure 6. The ±1 standard deviation error bars are derived from

222 the counting statistical uncertainties through uncertainty propagation. In only 3 of the 16 cases, the

223 individual measurements are more than one standard deviation from the mean PNAR Ratio. Thus, within

224 the precision of an individual measurement, each repeated measurement gives the same result.

225 **Table 2: PNAR Ratios measured from the same assembly after rotating it over 90 degrees.** The
226 means of the four measurements and the standard error of the means are listed.

Assembly	Rotation 1	Rotation 2	Rotation 3	Rotation 4	Mean
18	1.0401 ± 0.0012	1.0390 ± 0.0012	1.0407 ± 0.0012	1.0385 ± 0.0012	1.0396 ± 0.0005
28	1.0503 ± 0.0010	1.0510 ± 0.0011	1.0481 ± 0.0011	1.0464 ± 0.0012	1.0490 ± 0.0010
24	1.0454 ± 0.0012	1.0448 ± 0.0011	1.0440 ± 0.0013	1.0456 ± 0.0012	1.0449 ± 0.0004
42	1.0446 ± 0.0009	1.0460 ± 0.0010	1.0461 ± 0.0010	1.0452 ± 0.0009	1.0455 ± 0.0003

227

228 If it is assumed that the measurement uncertainty is independent of the measured assembly, information

229 from all 16 samples can be used to calculate a common, pooled standard deviation. The pooled

230 standard deviation is the best estimate of a single measurement uncertainty. For the four assemblies

231 repeatedly measured, the pooled standard deviation is 0.0013 and is shown in Figure 6 with dashed

232 lines.

233 The act of pulling the assembly out of the measurement position, rotating it and lowering it back subjects

234 the measurement to uncertainties caused by possible variations in the assembly positioning inside the

235 measurement position. However, an additional source of error could be introduced by the act of grabbing

236 the fuel assembly from its storage position and transporting it to the measurement area, e.g. from the

237 precision of the fuel transport machine positioning. Performing such truly independent repeated

238 measurements are left for a future measurement campaign.

Passive Neutron Albedo Reactivity Measurements of Spent Nuclear Fuel
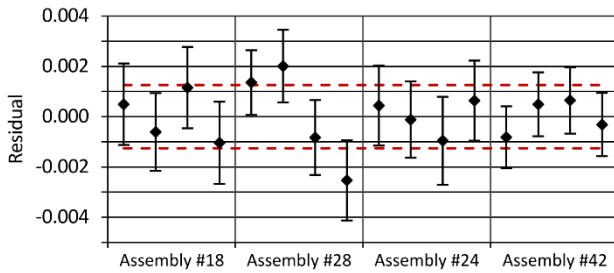
Figure 6: Deviation from the mean PNAR Ratio for the repeated measurements. The residual is the difference between a single measurement and the mean of the corresponding assembly. The error bars represent one standard deviation uncertainties of a single measurement due to counting statistics. The dashed lines are the ±1 pooled standard deviation for all four assemblies.
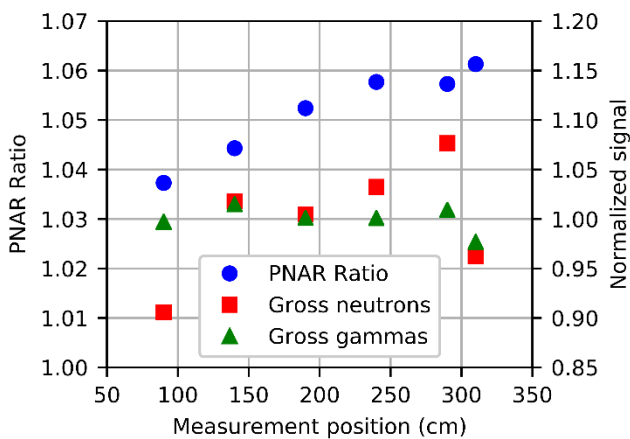
3.3   PNAR Signals at different measurement heights

Fuel assembly #4 was measured at 6 different heights. The selected assembly was a SVEA-64 design with only full-length rods and had an average initial enrichment of 3.0 %, an average burnup of 38 GWd/tU and a cooling time of 21 years. Figure 7 shows the PNAR Ratio and total neutron count rate and the gamma induced current in the ion chambers, both for the high multiplying scenario, at the different measurement heights. The neutron and gamma signals are normalized to the average of the datasets. The reported measurement position is from the bottom of the fuel assembly. The active length of a SVEA-64 assembly is 368 cm [15], which corresponds approximately to the interval between 30 cm and 400 cm in the measurement height. It is worth emphasizing that the neutron detectors are sensitive to an approximately 65 cm section of the fuel in a way that the sensitivity is greatest to the fuel segment at the axial level of the ^{3}He tubes and the parts of a measured fuel assembly outside this 65 cm section do not contribute to the measured PNAR Ratio [16]. The reported position in Figure 7 is the level of the neutron detectors. The gamma detectors are positioned 6.5 cm above the neutron detectors.

The neutron emission rate increases towards the top end of the assembly. During irradiation, the top part of a BWR assembly experiences lower moderator density than the bottom because of boiling. The harder energy spectrum leads to higher accumulation of actinides towards the top of the assembly. These include ^{244}Cm, the main isotope responsible for neutron generation in spent nuclear fuel through spontaneous fission. At both ends of the assembly, the burnup of the assembly decreases which causes neutron and gamma emission rates to decrease as well. The effect of burnup is more pronounced on neutron emission rate than on gammas. For spent fuel assemblies similar to the ones measured here, the neutron emission rate is dependent to between the third and fourth power of burnup, whereas the gamma emission rate is an approximately linear function of burnup [17]. This is seen also from our measurement results, where the neutron signal decreases more steeply than the gamma signal at the measurement points near both ends of the assembly.

268   The PNAR Ratio keeps increasing throughout the measurement range. SVEA-64 assemblies have no or

269   very modest axial profiling. Likely, the axial power profile experienced in BWR cores has depleted the

270   fuel more on the bottom half of the assembly leaving a reactivity distribution now seen with PNAR

271   measurements. Additionally, the isotopic composition, and the amount of neutron absorbers, differs

272   between the bottom and top parts of a spent fuel assembly due to the axial variation discussed in the

273   previous paragraph.

274   In addition to the SVEA-64 assembly discussed above, eight other assemblies were measured from two

275   heights. The difference in PNAR Ratio between the measurements is reported in Table 1. All these

276   assemblies contained partial length rods and the higher measurement position was chosen so that it

277   assays the area where partial length rods have ended. Four of these assemblies showed a greater than

278   three standard deviation increase in PNAR Ratio towards the top of the assembly, while one showed a

279   decrease of approximately two standard deviations. Based on the sample of nine assemblies, no clear

280   indication on which parameters affect this axial PNAR Ratio variation can be drawn.

281

282   **Figure 7: PNAR Ratio, gross gamma current and neutron count rate measured at different heights**

283   **of the same assembly (#4).** The gamma and neutron signals are normalized to their average values.

284   The measurement position is calculated from the bottom of the assembly.

285   **4   Discussion**

286   The distribution of the remaining fissile material and the neutron absorbers inside a spent BWR fuel

287   assembly can be very complex and variations between assemblies can be large. Before use, fresh

288   assemblies typically have both axial and horizontal initial enrichment profiling to compensate for

289   anticipated local moderator density changes within a reactor core. In modern fuel designs, partial length

290   rods are also used. During irradiation, multiple parameters affect the depletion of fissile material. These

291   include the assembly location inside the reactor core, the usage of control blades during operation, the

292   presence of burnable poisons, the power level history of the reactor and number and duration of reactor

293 outage periods. Furthermore, some assemblies may have been stored outside the reactor between
294 irradiation cycles for multiple years. As the fuel is irradiated, fission products and actinides accumulate in
295 the fuel assembly. Some of these isotopes are neutron absorbers. The multiplication assessed by PNAR
296 is affected by both; the depletion of fissile content and build-up of neutron absorbers.

297 The majority of the measured PNAR Ratios fall between 1.03 and 1.05. Assembly #5 stands out with a
298 PNAR Ratio of 1.088. This assembly has a relatively low burnup compared to its initial enrichment (i.e. it
299 is not fully irradiated). Compared to the other measured assemblies, it has more fissile content which is
300 also indicated by the larger PNAR Ratio. The average PNAR Ratio of the assemblies other than #5 is
301 1.044.

302 In Section 3.3, the PNAR Ratios measured at different heights of a fuel assembly were compared. For
303 roughly half of the measured assemblies, the PNAR Ratio measured at the upper part of the fuel
304 assembly was higher than that of the lower part. The axial variation of the PNAR Ratio seems to not be
305 only linked to fuel design as the highest difference was measured on an assembly with partial length
306 rods and the second highest with only full-length rods. It is expected that during final verification, each
307 assembly is measured once, at a fixed axial location.

308 With respect to the complex history of a spent fuel assembly, only its average initial enrichment, average
309 burnup and cooling time are typically declared, and these declaration parameters are the ones that are
310 then verified by NDA-measurements. Rather than directly verifying the declaration, PNAR Ratio
311 measurements could be used to screen assemblies for odd neutron multiplication to detect missing
312 fissile material. For our prototype design, an assembly having a PNAR Ratio e.g. lower than 1.03, could
313 be automatically flagged for an inspector review.

314 **4.1 Previous simulated PNAR responses**

315 Before the PNAR prototype was built, preliminary MCNP simulations were performed to quantify the
316 PNAR response to different fuel types. The simulation results are reported in [9,11] by Tobin et al. The
317 simulated assemblies had different initial enrichments and burnup values. For unirradiated assemblies,
318 the PNAR Ratios started at a value specific to the initial enrichment and they decreased as a function of
319 burnup. Independent of the initial enrichment, all assemblies reached the same PNAR Ratio for a burnup
320 resembling that of a fully irradiated assembly. Similarly, in our measurements, all the fully irradiated
321 assemblies had PNAR Ratios very close to each other, while the one partially irradiated assembly had a
322 significantly higher PNAR Ratio. However, the measured PNAR Ratios are systematically lower than
323 those predicted by the simulations.

324 The virtual assembly simulated in [11] closest to the measured assemblies had an initial enrichment of
325 3% and 20 years of cooling time. Figure 8 shows the reported simulated PNAR Ratios of this assembly

326   at burnups of 0, 15 and 30 GWd/tU. The simulated PNAR Ratio at 30 GWd/tU burnup is 1.149±0.003,

327   while the mean PNAR Ratio of the measured fully irradiated assemblies with 3.0% average initial

328   enrichment, also presented in Figure 8, was 1.0456. This difference between simulated and measured

329   PNAR Ratios is impacted by the fact that the assemblies used by Tobin et al. were not fully irradiated.

330   Instead, the virtual assemblies used were part of a parameters study (5% IE and 60 GWd/tU, 4% and 45

331   GWD/tU and 3% and 30 GWd/tU). The magnitude of this observation is evident in Table 1: the fully

332   irradiated commercial assemblies with an initial enrichment of 3.0%, other than the underirradiated

333   assembly #5, were irradiated on average, to a burnup of 35 GWd/tU. If the virtual assemblies would have

334   been irradiated to 35 GWd/tU, their PNAR Ratio would have been lower. Also, this difference was

335   affected by design differences between the simulated detector and the prototype one and simplifications

336   made in the numerical models.

337
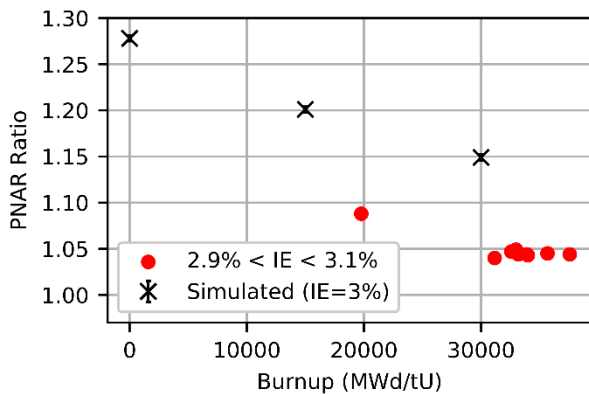
Figure 8: Simulated PNAR Ratios of a 3% initial enrichment assembly at different burnups [11]
**and measured PNAR Ratios of assemblies with similar enrichment.**

340   It is likely that a PNAR measurement is more sensitive to the fuel pins on the outer edges of a fuel

341   assembly, as the albedo neutrons are assaying the assembly from the outside. These pins are also the

342   ones that have been exposed to the greatest moderator density during reactor operation. Thus, the fuel

343   depletion is also increased in these pins compared to inner ones and such fuel nonuniformity was not

344   considered in the simulations reported in [9] and [11]. More realistic simulations to clarify the difference

345   in PNAR Ratios between simulations and measurements are needed as well as studies to quantify the

346   relative importance between inner and outer pins.

347   In the measurements, the decrease in the PNAR Ratio from a typical assembly to a non-multiplying

348   assembly, the dynamic range, is 1.044 – 0.97 = 0.074. Comparing the uncertainty of 0.0013, from

349   Section 3.2, quantified primarily by including the uncertainty in the assembly positioning in the detector

350   as well as counting statistics, we see that the magnitude of these two uncertainties is only ~2% of the

351   0.074 variation observed between a non-multiplying assembly and a typical fully irradiated assembly.

Passive Neutron Albedo Reactivity Measurements of Spent Nuclear Fuel

352 The main objective of a PNAR instrument is to verify that a spent fuel assembly contains fissile material.

353 Based on the small magnitude of the uncertainty caused by assembly positioning in the detector and

354 counting statistics, we conclude that the PNAR instrument as built can discern between a fully irradiated

355 assembly and an assembly not containing any fissile material with great certainty.

356 **4.2 Complementing PNAR and PGET measurements**
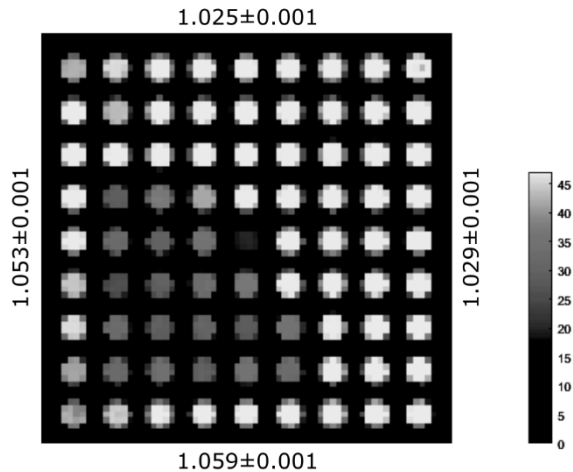
358 **Figure 9: PGET emission reconstruction of a 9x9-1 BWR assembly (#18) and PNAR Ratios of**

359 **individual pods.** The pod-specific PNAR Ratios are more sensitive to the fuel pins they are closest to.

360 During the PNAR measurements, PGET measurements were performed simultaneously for the same

361 fuel assemblies. Figure 9 presents one example of horizontal variation in BWR fuel identified with both

362 instruments. In the figure is a PGET emission reconstruction of a 9x9-1 fuel assembly (#18) from a

363 gamma ray energy window mainly sensitive to ^{137}Cs. The image reconstruction method used is

364 introduced in [18]. In PGET images, a higher emission value is linked to higher burnup. A local emission

365 drop can be identified in the lower left quadrant of the assembly. In Figure 9, around the PGET

366 reconstruction, are marked PNAR Ratios measured for the same assembly at the same time, that are

367 most sensitive to that particular side of the fuel assembly. Such signals are obtained by treating the

368 responses of each PNAR detector pod individually. Any discrepancies between detector pods were

369 averaged by performing four measurements where the assembly was rotated 90 degrees in between,

370 and thus, measuring each side of the assembly with each functioning detector pod. This also allowed for

371 measuring from the side with the malfunctioning detector pod. The side-specific PNAR Ratios indicate

372 similar results as the PGET reconstruction. The two pods further away from the emission drop show

373 significantly lower PNAR Ratios than the two pods closer to the drop. If the emission drop seen in the

374 PGET reconstruction is caused by a lower burnup, the same area should also have fractionally more

375 fissile material remaining inside the fuel, which is reflected by the higher specific PNAR Ratios closer to

376   that area. In addition to being an example of large horizontal variation within a fuel assembly, Figure 9

377   shows how PGET and PNAR results can be used to complement each other.

378   **5   Conclusions**

379   A new PNAR prototype instrument was used to measure the multiplication of BWR-type spent nuclear

380   fuel of various designs and reactor irradiation histories, thus verifying the presence of fissile content in

381   the fuel. The majority of spent fuel assemblies are expected to have similar PNAR Ratios between them,

382   as the reactor operators have strived to optimally extract the potential nuclear energy from each

383   assembly. All but one of the measured assemblies had a PNAR Ratio between 1.03 and 1.05. The one

384   atypical assembly that was significantly underirradiated given its initial enrichment and discharge burnup

385   had a PNAR Ratio of 1.088 which was clearly distinguishable from the other assemblies. Numerical

386   simulations have indicated that a non-multiplying assembly, that is an assembly in which no fission could

387   take place, would have a PNAR Ratio of approximately 0.97.

388   With repeated measurements, the total uncertainty caused by assembly positioning and counting

389   statistics of a single measurement was experimentally estimated to be 0.0013. This value is of the same

390   magnitude as the uncertainty calculated for counting statistics alone, indicating that counting statistics is

391   dominating the PNAR measurement uncertainty. However, experiments where the same fuel assembly

392   is repeatedly taken from the storage rack, moved to the measurement position and measured are

393   required to further quantify the measurement uncertainty. The measured PNAR Ratios were

394   systematically lower than previously reported simulated PNAR Ratios for virtual assemblies. Based on

395   reasons discussed in Section 4.1, this discrepancy seems to be caused by the final burnup choices of

396   the virtual assemblies and simplifications made in the numerical model.

397   Measurements from different heights of an assembly show that the PNAR Ratios from a single assembly

398   may vary significantly as a function of the axial position. Ultimately, this is caused by a complex

399   distribution of fissile isotopes in the spent fuel affected by assembly type, pin design, position in core,

400   void ratio, cooling time, etc. Usually the fuel parameters given in safeguards declarations are assembly

401   averages, making the choice of measurement position important when verifying the declaration based on

402   PNAR measurements. Yet, if the purpose of PNAR is to compare the multiplication among assemblies

403   and/or to detect that the multiplication is above some threshold, fixing the axial location of the

404   measurement is beneficial to minimizing the impact of this axial variation. Currently, each assembly is

405   expected to be measured only once, at one height, during the final verification.

406   By examining the PNAR responses of individual PNAR pods, horizontal variation in the multiplication of a

407   fuel assembly was identified. Similar patterns can be identified in PGET emission images. Comparing

408   the PNAR and PGET signals can be beneficial for understanding the verification results given by both

409   individual instruments.

410   PNAR was designed to complement the safeguards verification capabilities of PGET by verifying the

411   presence of fissile material, and to be able to collect the same signals as Fork devices, making a

412   combined PGET and PNAR measurement a powerful tool to verify spent fuel assemblies before their

413   final disposal. Based on the measurements performed and MCNP simulations, PNAR can discern

414   between an intact irradiated fuel assembly and a non-multiplying assembly with great confidence. The

415   one standard deviation estimate for the single measurement error was approximately 2% of the dynamic

416   range of the measurement. Furthermore, PNAR could be used to flag fuel assemblies of unnaturally low

417   multiplication for further analysis.

Acknowledgements

References

426   [1]   T. Honkamaa, M. Hämäläinen, E. Martikka, M. Moring, O. Okko, T. Tupasela, National Safeguards
427   Concept for Encapsulation Plant and Geological Repository, in: ESARDA 41st Annu. Meet. Symp.
428   Safeguards Nucl. Mater. Manag. 14-16 May 2019 Stresa Italy, ESARDA, Luxembourg, 2019: pp.
429   235–239. https://doi.org/doi:10.2760/159550.
430   [2]   T. White, T. Honkamaa, M. Mayorov, P. Peura, J. Dahlberg, J. Keubler, V. Ivanov, A. Turunen,
431   Application of Passive Gamma Emission Tomography (PGET) for the Verification of Spent Nuclear
432   Fuel, in: Proc. Inst. Nucl. Mater. Manag. Annu. Meet., Baltimore, MD, USA, 2018.
433   [3]   T. White, M. Mayorov, N. Deshmukh, E. Miller, L.E. Smith, J. Dahlberg, T. Honkamaa, SPECT
434   Reconstruction and Analysis for the Inspection of Spent Nuclear Fuel, in: 2017 IEEE Nucl. Sci.
435   Symp. Med. Imaging Conf. NSSMIC, IEEE, Atlanta, GA, USA, 2017.
436   https://doi.org/10.1109/NSSMIC.2017.8532776.
437   [4]   M. Mayorov, T. White, A. Lebrun, J. Brutscher, J. Keubler, A. Birnbaum, V. Ivanov, T. Honkamaa,
438   P. Peura, J. Dahlberg, Gamma Emission Tomography for the Inspection of Spent Nuclear Fuel, in:
439   2017 IEEE Nucl. Sci. Symp. Med. Imaging Conf. NSSMIC, IEEE, Atlanta, GA, USA, 2017.
440   https://doi.org/10.1109/NSSMIC.2017.8533017.
441   [5]   S. Vaccaro, I.C. Gauld, J. Hu, P. De Baere, J. Peterson, P. Schwalbach, A. Smejkal, A. Tomanin,
442   A. Sjöland, S. Tobin, D. Wiarda, Advancing the Fork detector for quantitative spent nuclear fuel
443   verification, Nucl. Instrum. Methods Phys. Res. Sect. Accel. Spectrometers Detect. Assoc. Equip.
444   888 (2018) 202–217. https://doi.org/10.1016/j.nima.2018.01.066.
445   [6]   D.M. Lee, L.O. Lindquist, Self-interrogation of spent fuel, 1982. https://doi.org/10.2172/6972434.
446   [7]   A.M. Bolind, Development of an analytical theory to describe the PNAR and CIPN nondestructive
447   assay techniques, Ann. Nucl. Energy. 66 (2014) 167–176.
448   https://doi.org/10.1016/j.anucene.2013.12.009.

449 [8] T. Tupasela, Passive neutron albedo reactivity assay of spent nuclear fuel, Master's Thesis, 2019.
450 http://urn.fi/URN:NBN:fi:aalto-201908254886.
451 [9] S.J. Tobin, P. Peura, C. Belanger-Champagne, M. Moring, P. Dendooven, T. Honkamaa, Utility of
452 Including Passive Neutron Albedo Reactivity in an Integrated NDA System for Encapsulation
453 Safeguards, ESARDA Bull. 56 (2018) 12–18.
454 [10] S.J. Tobin, P. Peura, C. Bélanger-Champagne, M. Moring, P. Dendooven, T. Honkamaa,
455 Measuring spent fuel assembly multiplication in borated water with a passive neutron albedo
456 reactivity instrument, Nucl. Instrum. Methods Phys. Res. Sect. Accel. Spectrometers Detect. Assoc.
457 Equip. 897 (2018) 32–37. https://doi.org/10.1016/j.nima.2018.04.044.
458 [11] S.J. Tobin, P. Peura, T. Honkamaa, M. Moring, C. Bélanger, Passive Neutron Albedo Reactivity in
459 the Finnish Encapsulation Context, 2018. http://urn.fi/URN:ISBN:978-952-309-406-2.
460 [12] S.J. Tobin, H.O. Menlove, M.T. Swinhoe, M.A. Schear, Next Generation Safeguards Initiative
461 research to determine the Pu mass in spent fuel assemblies: Purpose, approach, constraints,
462 implementation, and calibration, Nucl. Instrum. Methods Phys. Res. Sect. Accel. Spectrometers
463 Detect. Assoc. Equip. 652 (2011) 73–75. https://doi.org/10.1016/j.nima.2010.09.064.
464 [13] H.R. Trellue, M.L. Fensin, J.G. Richard, J.L. Conlin, S.J. Tobin, R.J. Kapernick, Description of
465 Irradiated UO2 Fuel Compositions Generated for NGSI Spent Fuel Libraries, Los Alamos National
466 Laboratory, 2011, LA-UR-11-00300.
467 [14] J.T. Goorley, M.R. James, T.E. Booth, J.S. Bull, L.J. Cox, J.W.Jr. Durkee, J.S. Elson, M.L. Fensin,
468 R.A.I. Forster, J.S. Hendricks, H.G.I. Hughes, R.C. Johns, B.C. Kiedrowski, R.L. Martz, S.G.
469 Mashnik, G.W. McKinney, D.B. Pelowitz, R.E. Prael, J.E. Sweezy, L.S. Waters, T. Wilcox, A.J.
470 Zukaitis, Initial MCNP6 Release Overview - MCNP6 version 1.0, 2013.
471 https://doi.org/10.2172/1086758.
472 [15] F. Sturek, L. Agrenius, Measurements of decay heat in spent nuclear fuel at the Swedish interim
473 storage facility, Clab, Svensk Kärnbränslehantering AB, 2006.
474 https://www.skb.se/publikation/1472024/.
475 [16] S.J. Tobin, T. Honkamaa, V. Litichevskyi, A. Turunen, C. Belanger-Champagne, M. Moring, P.
476 Dendooven, P. Peura, Passive Neutron Albedo Reactivity in an Integrated NDA System for
477 Encapsulation Safeguards, in: Proc. Inst. Nucl. Mater. Manag. Annu. Meet., Baltimore, MD, USA,
478 2018.
479 [17] D. Reilly, N. Ensslin, Hastings Smith, Jr., Passive Nondestructive Assay of Nuclear Materials, US
480 NRC, 1991, NUREG/CR-5550. https://www.lanl.gov/org/ddste/aldgs/sst-
481 training/Panda%20Manual%20Chapters.php.
482 [18] R. Backholm, T.A. Bubba, C. Bélanger-Champagne, T. Helin, P. Dendooven, S. Siltanen,
483 Simultaneous Reconstruction of Emission and Attenuation in Passive Gamma Emission
484 Tomography of Spent Nuclear Fuel, Inverse Probl. Imaging. 14 (2020) 317–337.
485 http://dx.doi.org/10.3934/ipi.2020014.
486